PNAS RESEARCH ARTICLE | GENETICS OPEN ACCESS

Cohesin ATPase activities regulate DNA binding and coiled-coil configuration

Xingya Xu[a,1], Ryuta Kanai[b], Li Wang[a], and Mitsuhiro Yanagida[a,2]

Contributed by Mitsuhiro Yanagida; received May 9, 2022; accepted July 6, 2022; reviewed by David Glover and Kerry Bloom

The cohesin complex is required for sister chromatid cohesion and genome compaction. Cohesin coiled coils (CCs) can fold at break sites near midpoints to bring head and hinge domains, located at opposite ends of coiled coils, into proximity. Whether ATPase activities in the head play a role in this conformational change is yet to be known. Here, we dissected functions of cohesin ATPase activities in cohesin dynamics in *Schizosaccharomyces pombe*. Isolation and characterization of cohesin ATPase temperature-sensitive (ts) mutants indicate that both ATPase domains are required for proper chromosome segregation. Unbiased screening of spontaneous suppressor mutations rescuing the temperature lethality of cohesin ATPase mutants identified several suppressor hotspots in cohesin that located outside of ATPase domains. Then, we performed comprehensive saturation mutagenesis targeted to these suppressor hotspots. Large numbers of the identified suppressor mutations indicated several different ways to compensate for the ATPase mutants: 1) Substitutions to amino acids with smaller side chains in coiled coils at break sites around midpoints may enable folding and extension of coiled coils more easily; 2) substitutions to arginine in the DNA binding region of the head may enhance DNA binding; or 3) substitutions to hydrophobic amino acids in coiled coils, connecting the head and interacting with other subunits, may alter conformation of coiled coils close to the head. These results reflect serial structural changes in cohesin driven by its ATPase activities potentially for packaging DNAs.

cohesin | ATPase | suppressor screen | DNA binding | coiled coil

Significance

Cohesin is a heteropentameric protein complex consisting of two structural maintenance of chromosomes (SMC) subunits and three non-SMC subunits. The two SMC subunits form a heterodimer with an ATPase head and hinge that are connected by long coiled coils. Isolation of ATPase mutants followed by comprehensive identification of suppressor mutations in SMC subunits that can bypass ATPase defects was performed. Locations and properties of mutant alleles reflect how ATPase activities could be compromised by structural adaptation. ATP-driven conformational changes may enhance DNA anchoring by the head, alter interactions of coiled coils at the head with other subunits for DNA to go through, and fold/extend coiled coils near break sites around midpoint to bring together DNA elements far from each other.

The cohesin complex is required for sister chromatid cohesion, DNA damage response, gene expression, and spatial organization of the genome (1, 2). Psm1/SMC1 and Psm3/SMC3 form a stable heterodimer via both hinge–hinge interaction and ATPase heads engagement upon ATP binding (3–5). Cohesin owns two ATPase domains at its globular head. Each ATPase domain contains the Walker A and Walker B consensus sequences found in most ATPases (5, 6) and several other sequence motifs, such as signature motif and D loop (7). Both ATPase domains are required for efficient loading of cohesin (8). Rad21/SCC1, the kleisin subunit with its N-terminal domain, interacts with Psm3/SMC3 coiled coils (CCs) emerging from the head, and its C-terminal domain interacts with Psm1/SMC1 head domain (9–12). Psc3/SCC3 associates with the unstructured region in the middle of Rad21/SCC1 (13–15).

Mis4/SCC2/NIPBL functions as the cohesin loader (16, 17). Mis4/SCC2/NIPBL forms a harp-shaped structure (18, 19). Its N-terminal domain binds to Psm3/SMC3 coiled coils close to the head domain and its C-terminal domain binds to Psm1/SMC1 coiled coils close to the head domain (11, 15). Mis4/SCC2/NIPBL also stimulates cohesin's ATPase activity for efficient cohesin loading (20–22).

All coiled coils of SMC complexes (cohesin, condensin, and SMC5-SMC6 complex) are ~50 nm long and are essential for their functions (23–25). SMC coiled coils contain interruptions (break sites hereafter) that disrupt the characteristic seven-residue amino acid sequence repeats, known as heptad repeats (26, 27). It has been proposed that cohesin folds around the midpoints of its coiled coils to bring the head and hinge domains into proximity (20, 28–30). However, it is still unclear how such molecular architecture of cohesin works to fulfill its function. In this study, we isolated temperature-sensitive (ts) mutants with single amino acid substitutions in the signature motif or D loop of cohesin ATPase domains, which presumably impair ATPase activity of cohesin. Then, screening of suppressor mutations that rescued the lethality caused by ATPase defects identified several hot regions in cohesin SMC subunits, which are involved in DNA binding, interaction with non-SMC subunits, or coiled-coil dynamics around midpoints. Therefore, these results coupled the dynamics of the cohesin complex with ATPase activity.

Author contributions: X.X. and M.Y. designed research; X.X. and L.W. performed research; X.X., R.K., and M.Y. analyzed data; and X.X., R.K., and M.Y. wrote the paper.

Reviewers: D.M.G., Division of Biology and Biological Engineering, California Institute of Technology; and K.S.B., University of North Carolina at Chapel Hill.

The authors declare no competing interest.

[1]Present address: Institute of Future Agriculture, Northwest A&F University, Yangling, Shaanxi 712100, China.

[2]To whom correspondence may be addressed. Email: myanagid@gmail.com.

This article contains supporting information online at http://www.pnas.org/lookup/suppl/doi:10.1073/pnas.2208004119/-/DCSupplemental.

Published August 8, 2022.

Results

Isolation of Cohesin ATPase Temperature-Sensitive Mutants. Multiple in vitro ATPase activity experiments indicated that mutations in the signature motif or D loop of ATP-binding cassette (ABC) ATPase domains caused lower or loss of ATPase activity (10, 31–34). To understand how ATPase domains regulate cohesin dynamics, we selected four consecutive amino acids in the highly conserved signature motif and one leucine residue in the D loop of both Psm1/SMC1 and Psm3/SMC3 ATPase domains (indicated by red arrowheads) for targeted random mutagenesis in fission yeast *Schizosaccharomyces pombe* (*S. pombe*) (Fig. 1*A*). Synthetic oligonucleotides were designed for each of the 10 amino acids to introduce all kinds of potential single amino acid substitutions. After screening ∼2,200 integrants, we obtained five ts mutants (Fig. 1*B*). Four (Psm1-L1132T, Psm3-L1097P, Psm3-S1098A, and Psm3-G1100A) of the five responsible mutations were located in signature motifs (or C motifs) and the other one (Psm1-L1166N) in the Psm1 D loop (Fig. 1*C*). Temperature sensitivity of *psm3-S1098A* and *psm1-L1166N* was confirmed by reintegrating the responsible mutations into wild-type strain. Both signature motifs of the head domains are located at the dimeric interface and the signature motif of one SMC subunit forms the ATP binding site together with the Walker A motif of the other SMC subunit (11). All mutations in signature motifs of Psm3/SMC3 (L1097P, S1098A, and G1100A) and Psm1/SMC1 (L1132T) would destabilize the ATP binding surface by steric hindrance or local structural changes, resulting in decreased ATPase activity.

We reintegrated the Psm3-S1098A ts mutation into a strain, in which histone H2A was tagged with RFP, and α-tubulin Atb2 and a spindle pole body protein Sid4 were tagged with GFP (35). Mitotic chromosome segregation defects were observed at restrictive temperature (36 °C) (Fig. 1*D*). Then, *psm3-S1098A* and *psm1-L1166N* mutant cells, cultured at the restrictive temperature (36 °C) and the permissive temperature (26 °C), were observed under fluorescent microscopy after DAPI staining. Approximately 60% of the analyzed mitotic cells in the cohesin ATPase ts mutants exhibited chromosome missegregation phenotypes at restrictive temperature, while the frequency is less than 20% at the permissive temperature (Fig. 1*E*). These results indicate that activities from both cohesin ATPase domains are required for cohesin to fulfill its functions in proper chromosome segregation.

Spontaneous Mutations Rescuing ATPase Temperature-Sensitive Mutants. Spontaneous suppressor screening is a powerful and unbiased tool to identify second mutation (suppressor mutation) that can bypass the lethality (functional defects) caused by the temperature-sensitive mutation. To reveal the functional effects of cohesin ATPase domains, spontaneous suppressor screens were performed for three cohesin ATPase ts mutants (*psm3-S1098A*, *psm1-L1132T*, and *psm1-L1166N*) at restrictive temperature (Fig. 2*A*) (36). Next-generation sequencing identified a number of suppressor mutations in genes encoding either SMC subunit of cohesin (Psm1/SMC1 or Psm3/SMC3). They are presented in *SI Appendix*, Table S1 and their relative locations in Psm1/SMC1 and Psm3/SMC3 were shown in Fig. 2 *B* and *C*. From the data we realized that suppressor mutations are enriched in cohesin ATPase head domains, head coiled-coil junctions, and some regions of coiled coils.

Localization of potential coiled-coil domains in Psm1/SMC1 and Psm3/SMC3 was predicted by MARCOIL (37) and are shown as coiled-coil probability (Fig. 2 *B* and *C*). Locations with reduced coiled-coil probability scores indicate potential break sites in Psm1/SMC1 and Psm3/SMC3 coiled coils (red arrowheads in Fig. 2 *B* and *C*). Surprisingly, suppressor mutations of *psm3-S1098A* and *psm1-L1166N* that are mapped to coiled coils of Psm1/SMC1 and Psm3/SMC3 are enriched in or close to these break sites. Therefore, the cohesin ATPase activities seem to have relevant functions in regulating coiled-coil dynamics at break sites around midpoints.

Comprehensive Targeted Suppressor Identification. To understand the properties of the suppressor mutations and how they affect cohesin dynamics to compensate for cohesin ATPase defects, several regions (Psm3-HCJ, Psm3-CCN, Psm1-CCN, and Psm3-BS) that are enriched in suppressor mutations, but are not in cohesin ATPase domains, were selected for comprehensive targeted suppressor screening using saturation mutagenesis (Fig. 2 *B* and *C*). Locations of Psm3-HCJ, Psm3-CCN, Psm1-CCN, and Psm3-BS in cohesin were illustrated (Fig. 2 *D* and *E*). Psm3/SMC3 head-coiled coil junction (Psm3-HCJ, amino acids 95∼130) may bind DNA (Fig. 2*E*). Psm3/SMC3 coiled coil emerging from N-terminal head domain (Psm3-CCN, amino acids 181∼200) and Psm1/SMC1 coiled coil emerging from N-terminal head domain (Psm1-CCN, amino acids 179∼202) interact with Rad21N and Mis4C, respectively (Fig. 2*E*), and a Psm3/SMC3 break site in N-terminal coiled coil (Psm3-BS, amino acids 295∼350) is far from the cohesin ATPase head domain (Fig. 2*D*).

In a previous study, a spontaneous suppressor screen for a ts mutant *rad21-I67F*, which contains a I67F mutation at the Rad21 N-terminal domain that was predicted to destabilize the interaction between Rad21N and Psm3 coiled coil, identified mutations in cohesin ATPase domains (30). Here, we crossed *psm3-G1100A* and *psm1-L1132T*, isolated in this study, with *rad21-I67F* and found that they can rescue the *rad21-I67F* ts mutant partially (*SI Appendix*, Fig. S1*A*). Therefore, loss of cohesin ATPase activity rescues the *rad21-I67F* ts mutant. We proposed that suppressors of cohesin ATPase ts mutants (*psm3-S1098A* and *psm1-L1166N*) may mimic the effects of cohesin ATPase activities, while suppressors of *rad21-I67F* may mimic cohesin ATPase defects (*SI Appendix*, Fig. S1*B*).

In summary, targeted suppressor screens followed the procedure described in *SI Appendix*, Fig. S1*C* and targeted sequencing identified 455 single amino acid substitutions in these hotspots from ∼1,600 revertants isolated at restrictive temperatures (*SI Appendix*, Fig. S1*D*).

We compared suppressor mutations of *psm3-S1098A* in Psm3-BS obtained independently from spontaneous suppressor screening and targeted suppressor screening. Five of the six spontaneous suppressors mapped in Psm3-BS were identified in targeted suppressor screening too (*SI Appendix*, Fig. S2*A*). In addition, two independent targeted suppressor screens were performed in Psm3-CCN for comprehensiveness (*SI Appendix*, Fig. S2*B*). Suppressor mutations identified in the first and second screens are highly overlapped (*SI Appendix*, Fig. S2*C*). Therefore, the results supported suppressions of the ts mutants as indeed caused by the suppressor mutations identified in the targeted suppressor screens performed in this study.

Suppressor Mutations in the Head Lie in a DNA Binding Domain. Psm3-HCJ binds DNA and interacts with Rad21N (Fig. 3*A*) (11). Single amino acid substitutions in Psm3-HCJ that were identified as suppressors of *psm3-S1098A* or *rad21-I67F*, were shown in Fig. 3*B*. Indeed, suppressor mutations of *psm3-S1098A* and *rad21-I67F* were not overlapped at all. Among

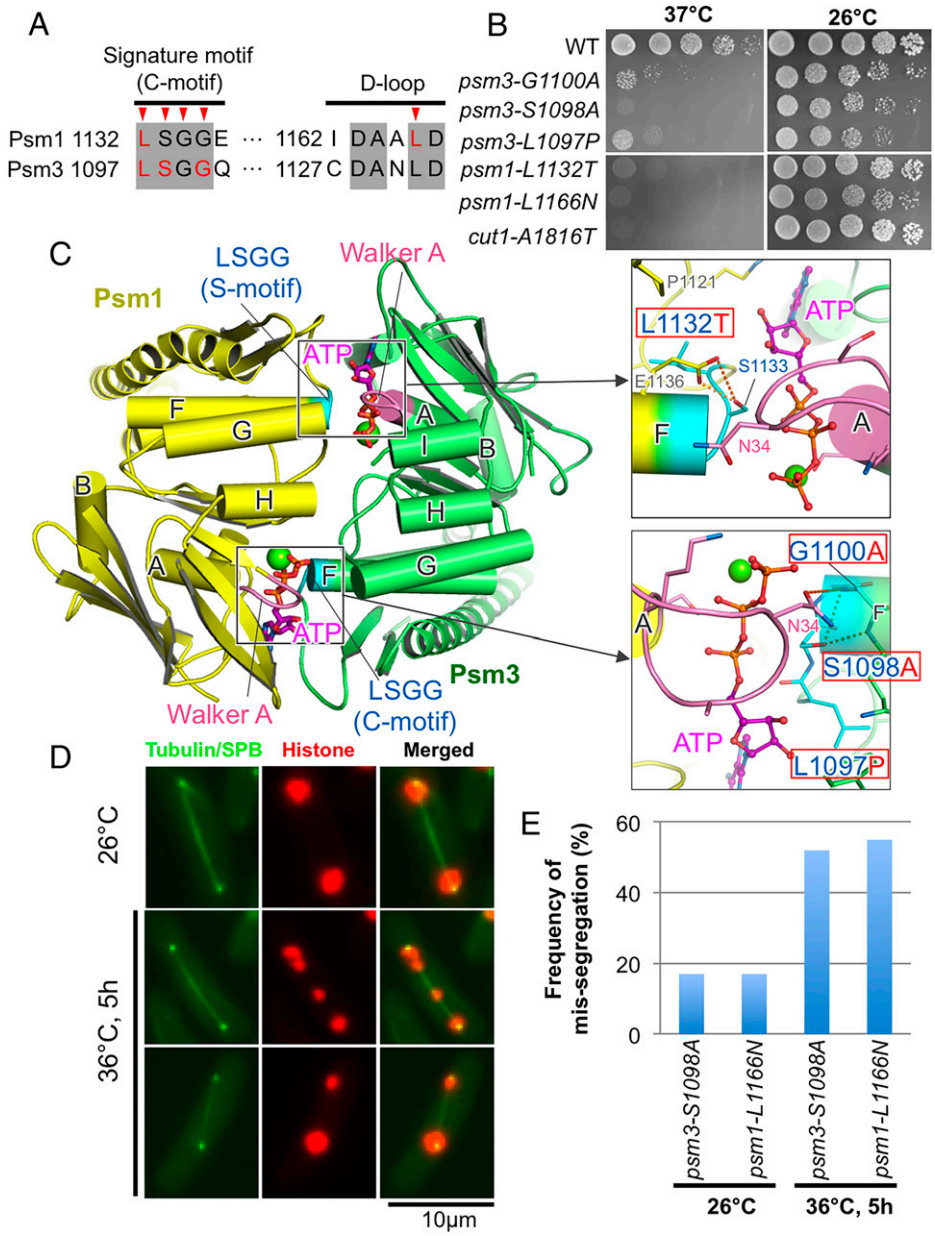

Fig. 1. Cohesin ATPase ts mutants. (*A*) Alignment around signature motifs and D loops of *S. pombe* cohesin ATPase domains. Amino acids selected for mutagenesis are indicated by red arrowheads. Amino acids involved in the ts mutants are colored red. (*B*) Spot test results of the five ATPase ts mutants. (*C*) Structual details of the signature motifs (PDB code: 6YUF). ATP molecules were built based on the cryogenic electron microscopy structure of the ATP-bound cohesin complex (PDB code: 6ZZ6). The signature and Walker A motifs are colored in cyan and violet, respectively. Mg^{2+} ions are shown as lime spheres. Hydrogen bonds are represented with dashed lines. Helices in the head are shown as cylinders. The backbone of the signature motif runs along the triphosphate group of adenosime triphosphate (ATP) to form its binding surface. The side chains of leucine and serine residues in the signature motif stabilize the ATP binding surface with hydrogen bonds or hydrophobic interactions. (*D*) Chromosome missegregation phenotypes observed in *psm3-S1098A*. (*E*) Frequency of chromosome missegregation events.

psm3-S1098A suppressors, arginine (R) was frequently observed in mutant alleles. Substitutions to arginine in *psm3-S1098A* suppressors lie in a region of the head close to DNA in the cohesin complex; therefore, they may enhance the DNA binding ability of Psm3-HCJ by establishing new electrostatic interactions with DNA (Fig. 3 *C* and *D*).

Four amino acid residues in Psm3-HCJ (D107, S117, K118, and T119) make direct contact with DNA (Fig. 3*B*). Among *rad21-I67F* suppressors, Psm3-K118 is frequently mutated to other amino acids (Fig. 3*B*), as 12 distinct single amino acid substitutions were obtained at Psm3-K118. Lys118 of Psm3/SMC3 is the unique residue in Psm3-HCJ that forms a salt bridge with DNA (Fig. 3*E*); the suppressor mutations of *rad21-I67F* at Psm3-K118 would result in less interaction of Psm3-HCJ with DNA.

Many Suppressors in Coiled Coils Near the Head Lie in or near Regions Associated with Other Subunits. Psm1-CCN interacts with the Mis4/SCC2/NIPBL C terminus and Psm3-CCN interacts with the Rad21/SCC1 N terminus (Fig. 4*A*) (11). Spontaneous suppressors of Psm1/SMC1 ATPase ts mutants (*psm1-L1132T* and *psm1-L1166N*) were enriched in Psm1-CCN, while spontaneous suppressors of *rad21-I67F* were enriched in Psm3-CCN (Fig. 2 *B* and *C*). Single amino acid substitutions, identified from targeted saturation mutagenesis, as suppressors of *psm1-L1166N* in Psm1-CCN or of *rad21-I67F* in Psm3-CCN are presented (Fig. 4 *B* and *C*).

To understand hydrophobicity tendency of mutated residues, we counted the frequency of each of the 20 amino acids in mutant alleles involved in the single amino acid substitutions

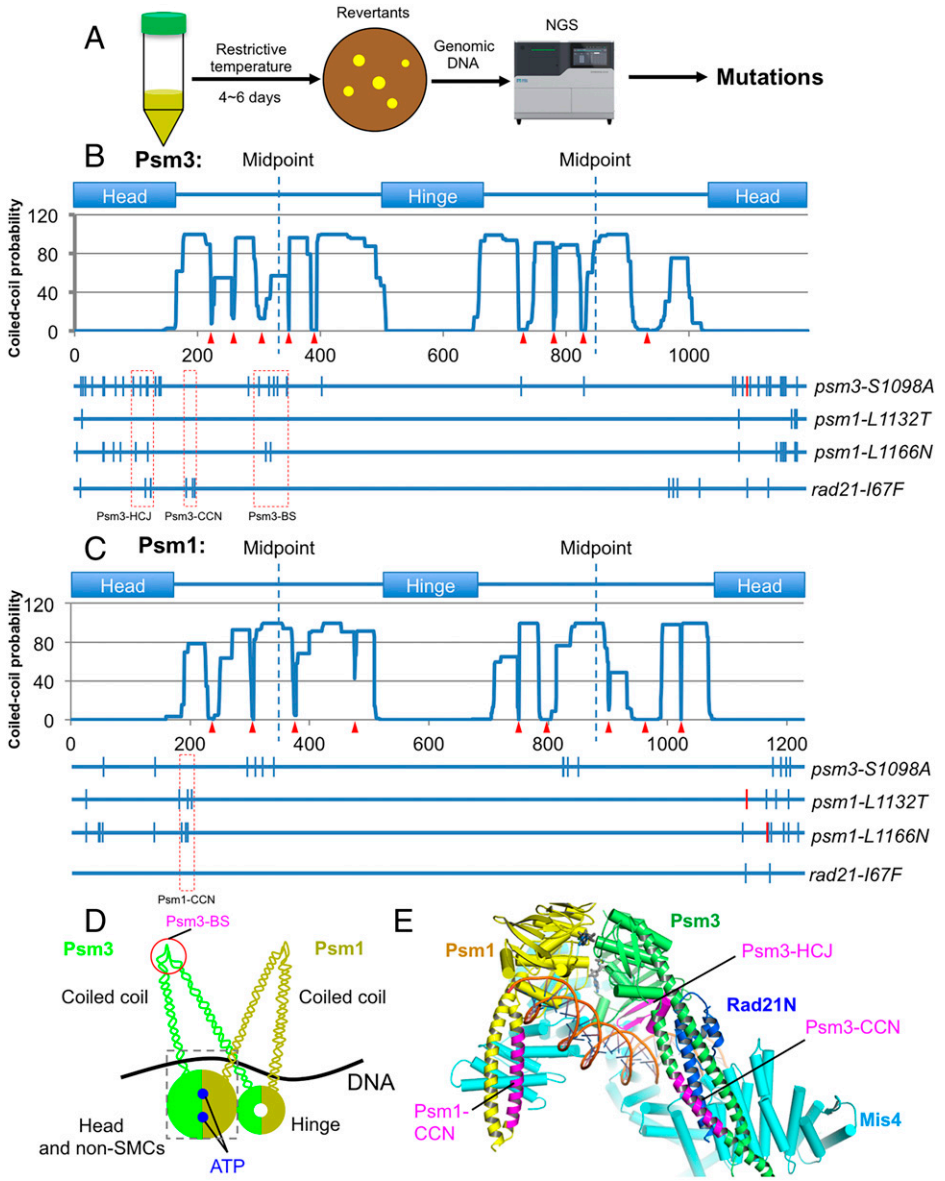

Fig. 2. Suppressor mutations in cohesin SMC subunits. (*A*) A strategy to identify spontaneous suppressor mutations for the ATPase ts mutants. (*B* and *C*) Location of suppressor mutations of cohesin ATPase ts mutants or *rad21-I67F* identified in Psm3/SMC3 (*B*) and Psm1/SMC1 (*C*), are indicated by vertical bars. Locations of suppressor hotspots (Psm3-HCJ, Psm3-CCN, Psm1-CCN, and Psm3-BS), selected for targeted saturation mutagenesis, are indicated by red dashed rectangles. Potential break sites are indicated by red arrowheads. (*D*) A cartoon exhibiting a folded form of the cohesin complex. Position of Psm3-BS is indicated. (*E*) Structural view of the targeted regions (magenta) that were selected for saturation mutagenesis.

(Fig. 4 *D* and *E*). Compared to hydrophilic amino acids, hydrophobic amino acids are enriched in mutant alleles in both Psm1-CCN (Fig. 4*D*) and Psm3-CCN (Fig. 4*E*).

Suppressors of *psm1-L1166N* in Psm1-CCN locate at the positions facing either Mis4/SCC2/NIPBL or Psm1 CC_C, and these suppressors seem to affect the interaction with Mis4/SCC2/NIPBL directly or indirectly through changing intra-association between CC_N and CC_C of Psm1/SMC1 (Fig. 4*F*). Suppressors of the *rad21-I67F* ts mutant in Psm3-CCN locates at positions either having van der Waals interactions with Rad21N or forming tight interactions with Psm3 C-terminal coiled coil (Fig. 4*G*). These suppressors in Psm3-CCN are predicted to repair the improper subunit interaction between Rad21/SCC1 and Psm3/SMC3 caused by I67F mutation.

How cohesin ATPase activities regulate interaction between coiled coils emerging from the head with associated non-SMC subunits is still unclear. Cohesin ATPase activities may induce structural changes at the head, which alters coiled coils' orientations at the head and affects non-SMC subunits' association with coiled coils at the head (Fig. 4*H*).

Coiled-Coil Mutations at a Break Site Are Supposed to Affect Coiled-Coil Probability. Psm3-BS contains eight heptad repeats (designated HR1~HR8). Among the 186 single amino acid substitutions identified in Psm3-BS for *psm3-S1098A*, 122 mutations locate in the first four heptad repeats (HR1~HR4), while the other 64 mutations locate in the last four heptad repeats (HR5~HR8); therefore, the first four heptad repeats (HR1~HR4) contain many more mutations than the last four heptad repeats (HR5~HR8) (Fig. 5*A*). HR1~HR4 have much lower coiled-coil probability than HR5~HR8 (Fig. 5*B*). Mutation frequency and coiled-coil probability in Psm3-BS are inversely correlated.

We compared molecular weights of mutant alleles with their corresponding wild-type alleles and calculated mean relative molecular weights (MWs) for each amino acid position and

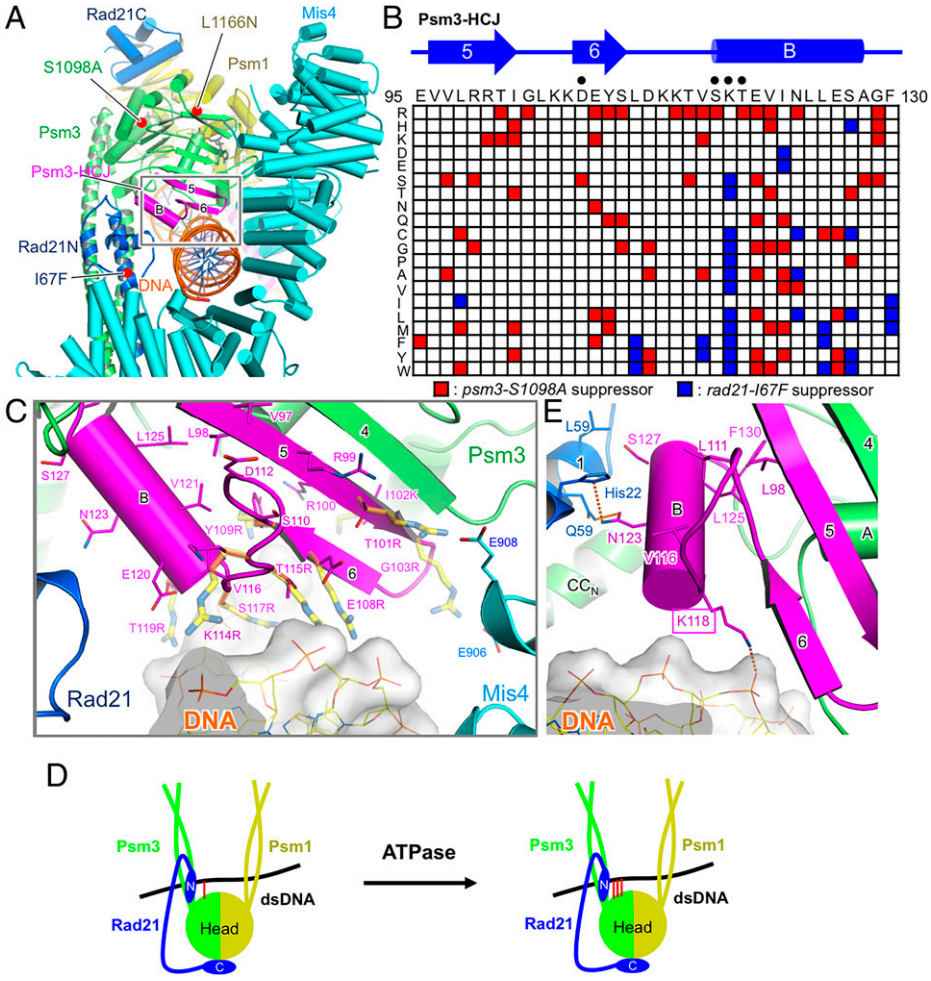

Fig. 3. ATPase activities affect DNA binding by head. (*A*) Structural view of Psm3-HCJ (magenta). (*B*) Single amino acid substitutions that were identified as suppressors of *psm3-S1098A* (red) or *rad21-I67F* (blue) in Psm3-HCJ. Columns depict positions along the primary sequence, and rows indicate a mutation to one of the 20 amino acids. Amino acids that may bind DNA are indicated by "•." (*C*) Structural detail of the suppressor sites of *psm3-S1098A* in Psm3-HCJ (magenta). Sticks in Psm3-HCJ represent the suppressor sites. Arg/Lys mutations identified as the suppressors are manually modeled and shown in yellow transparent sticks. (*D*) A cartoon exhibiting that cohesin ATPase activities may enhance the head's interaction with DNA. Interactions between the head and DNA are indicated by red bars. (*E*) Structural view of Psm3-K118's interaction with DNA.

plotted those against their positions in Psm3-BS. Surprisingly, a negative value of mean relative MW was obtained at most of the positions in Psm3-BS (Fig. 5*C*), indicating that *psm3-S1098A* suppressors in Psm3-BS tend to replace wild-type amino acids with other amino acids having smaller side chains.

Then coiled-coil probabilities were calculated for each substitution in Psm3-BS using the mutant Psm3/SMC3 protein sequences (37). A mean relative CC probability value at each amino acid position was calculated by comparing coiled-coil probabilities of mutant alleles with the coiled-coil probability of the wild-type allele. Mean relative CC probabilities were plotted against their positions in Psm3-BS (Fig. 5*D*). Most single amino acid substitutions in Psm3-BS tend to reduce the coiled-coil probability of Psm3-BS.

SI Appendix, Fig. S3*A* presents a heptad repeat showing how positions a–g appear when viewed from the top of an antiparallel helix. Residues at "a" and "d" are hydrophobic, forming a hydrophobic core between helices. Residues at "e" and "g" are charged residues forming ion pairs (38). We aligned sequences in HR5, HR6, and HR7 according to amino acid positions in a heptad repeat. Numbers of single amino acid substitutions at each position were plotted against their positions (*SI Appendix*, Fig. S3*B*). Most single amino acid substitutions occurred at core residues (a, d, e, and g), which are critical in maintaining helix–helix interactions in the coiled coil. The suppressor mutations probably tend to destabilize the interactions.

The suppression of cohesin ATPase ts mutants by mutations in coiled coils at the break site indicates that cohesin ATPase activities may regulate coiled-coil probabilities at break sites. Since break sites in coiled coils are located around midpoints far from the ATPase head, how cohesin ATPase activities regulate coiled-coil probabilities around break sites is still unclear. Cohesin ATPase activities may induce structural changes at the head, which may be propagated to coiled coils and reduce coiled-coil probabilities at break sites. Therefore, cohesin ATPase activities may regulate coiled-coil folding and/or extension (Fig. 5*E*).

Discussion

The functions of the cohesin complex in sister chromatid cohesion have been well studied (1, 2). The cohesin complex has been proposed to form a ring-shaped structure (39), in which the globular ATPase head domain and hinge domain are 50 nm away in distance, connected by long coiled coils (4, 40); chromosomal DNAs are topologically entrapped in the ring (21, 41, 42). In anaphase, activated Cut1/separase cleaves Rad21/SCC1 to open the cohesin ring to release chromosomal DNAs inside (43–46). Recently, a folded conformation of cohesin molecules about

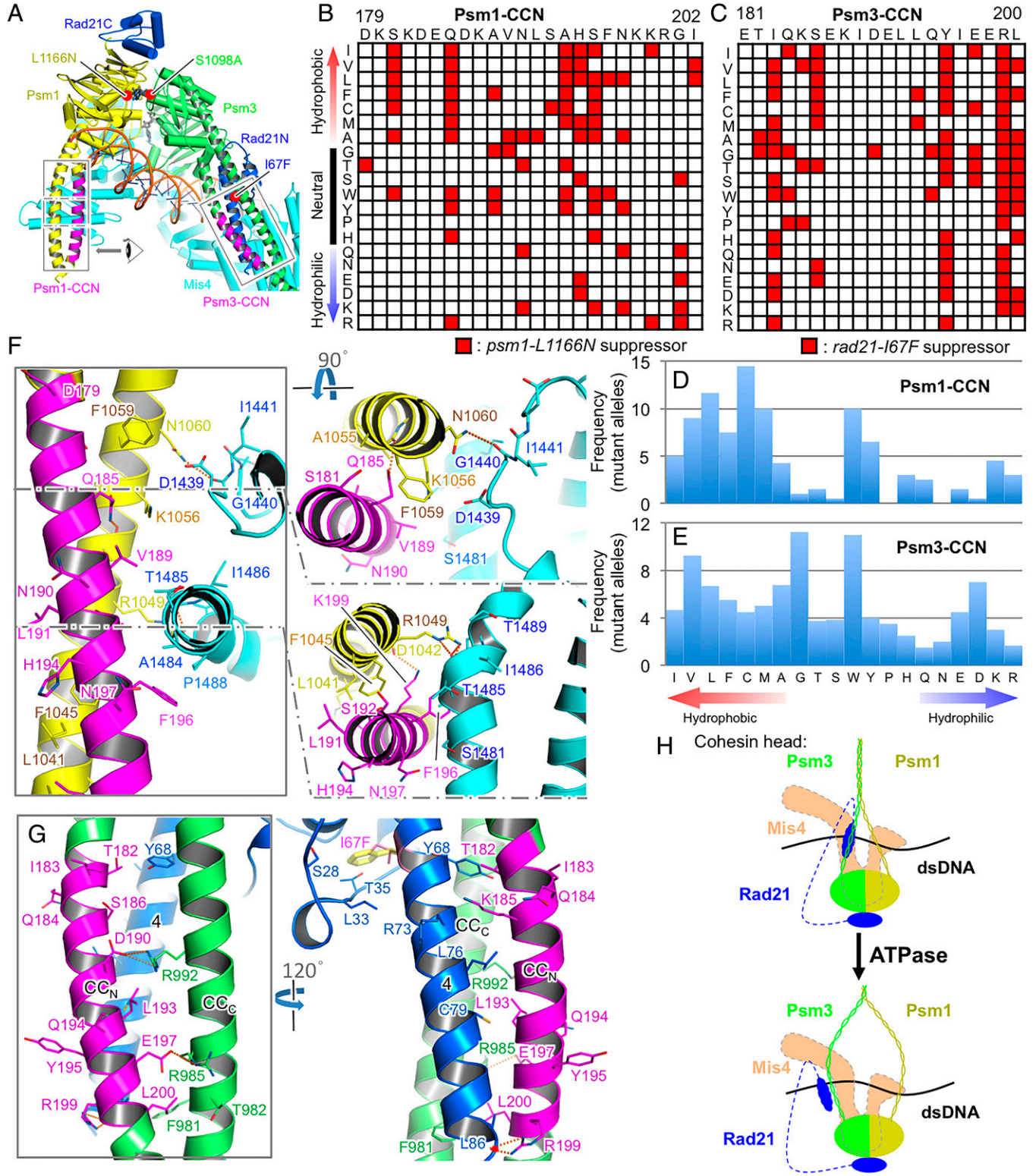

Fig. 4. ATPase activities affect coiled-coil interactions with associated subunits at the head. (*A*) Structural view of Psm1-CCN and Psm3-CCN (PDB code: 6YUF). (*B* and *C*) Data matrices presenting single amino acid substitutions that were identified as suppressors of *psm1-L1166N* in Psm1-CCN (*B*) and suppressors of *rad21-I67F* in Psm3-CCN (*C*). (*D* and *E*) Frequency of the 20 amino acids in mutant alleles obtained in Psm1-CCN (*D*) and Psm3-CCN (*E*). (*F*) Structural view of *psm1-L1166N* suppressors in Psm1-CCN. The suppressing residues and the ones interacting with these suppressing residues are represented by sticks. Hydrogen bonds and salt bridges are shown in orange broken lines. (*G*) Structural view of *rad21-I67F* suppressors in Psm3-CCN. I67 of Rad21/SCC1 faces inside the N-terminal domain of Rad21/SCC1 to form a hydrophobic core with A20, S28, L33, and T35 near the interface with Psm3-CCN. (*H*) A cartoon exhibiting that cohesin ATPase activities may drive a change in coiled-coil orientation at the head.

25 nm in length was also observed with atomic force microscopy (40, 47) and electron microscopy (20, 28). Coiled coils contain interruptions around their midpoints (27, 28, 48). Cohesin coiled coils were supposed to fold around midpoints to bring head and hinge domains into proximity (28, 30, 49), and much work has been done to detect coiled-coil folding (28, 50, 51).

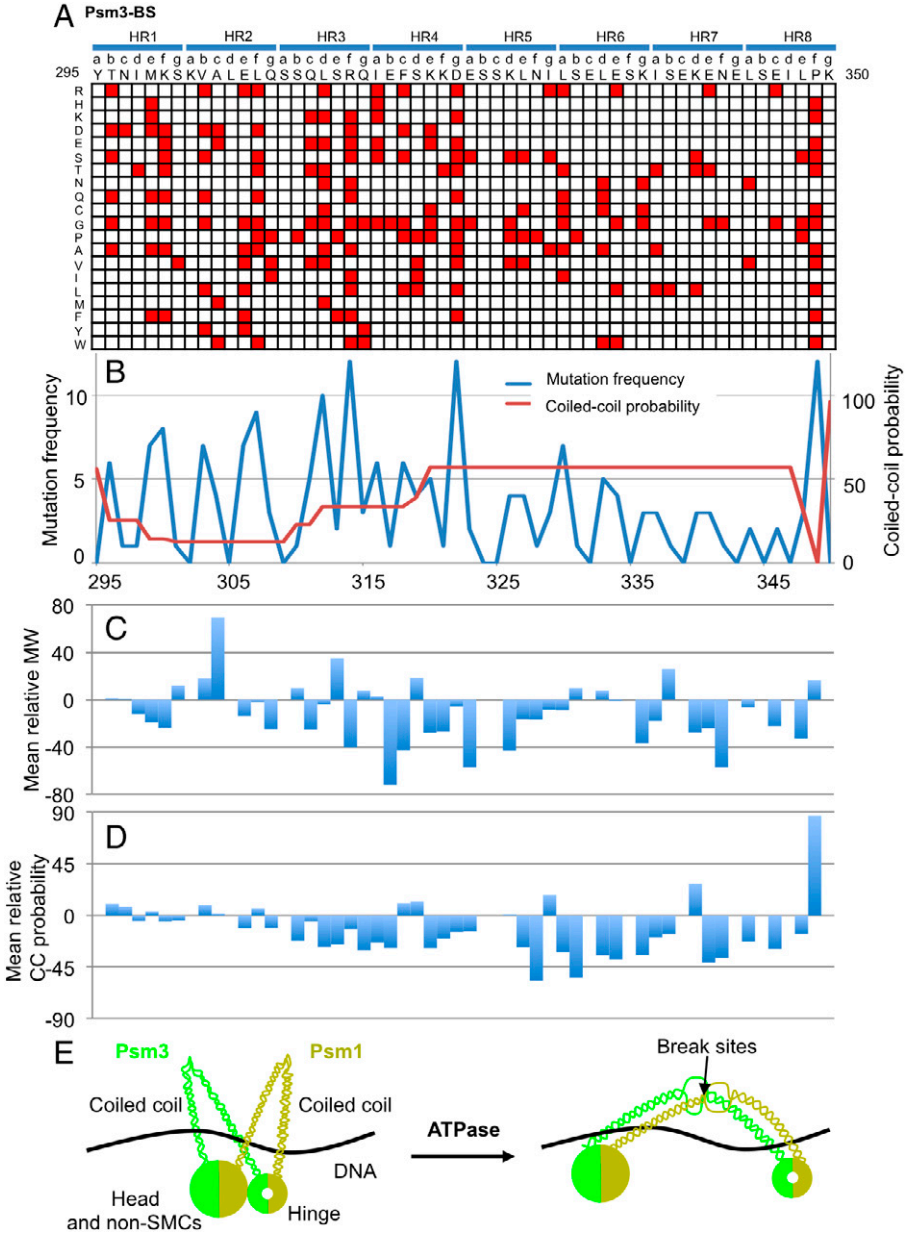

Fig. 5. Suppressors around a coiled-coil break site. (*A*) Data matrix showing single amino acid substitutions in Psm3-BS that rescue the temperature sensitivity of *psm3-S1098A*. The eight heptad repeats predicted by MARCOIL are shown above the primary sequence. (*B*) Numbers of single amino acid substitutions versus coiled-coil probability. (*C*) Mean relative molecular weight. (*D*) Mean relative coiled-coil probabilities. (*E*) A cartoon exhibiting that cohesin ATPase activities may regulate coiled-coil folding and extension at break sites.

Mis4/SCC2/NIPBL and Psc3/SCC3 were supposed to mediate interaction between head and hinge too (11, 15, 21, 52). Coiled coils can align and zip up (53), which is reminiscent of the Mre11-Rad50 complex. Upon DNA binding, the two coiled coils of Rad50 zip up into a rod (54). Cohesin probably held and released DNA through the actions of coiled coils (30, 50).

Except for its fundamental role in sister chromatid cohesion, cohesin is also required to shape three-dimensional genome architecture (55). Cohesin organizes the genome via DNA loop extrusion (29, 56, 57). Single-molecule imaging provided direct evidence that the cohesin complex extrudes DNA loops in vitro, and loop formation and extrusion requires cohesin's ATPase activity (20, 58). In addition, folding and extension of cohesin coiled coils were supposed to have a role in DNA looping (28, 29) and holding sister chromatids together (51). Cohesin coiled coils are supposed to transfer ATP binding/hydrolysis signals generated in the head to the hinge domains (24). Therefore, extension of the folded coiled coils may require energy released from ATP hydrolysis.

In this study, we identified single amino acid substitutions in *S. pombe*, which either rescued the cohesin ATPase defects or caused the same defects as cohesin ATPase mutants, through unbiased spontaneous genetic screens followed by targeted comprehensive genetic screens. Distribution and characteristics of the single amino acid substitutions indicate the functional effects of cohesin ATPase activity in cohesin structure, thereby helping us to dissect the conformational changes driven by cohesin ATPase activities: 1) Some of cohesin ATPase mutants' suppressor mutations were mapped in DNA binding domains in the Psm3/SMC3 head (Psm3-HCJ); mutational analysis indicated that they may enhance cohesin's interaction with DNA. Therefore cohesin ATPase activities may cause structural changes at the head to grip DNA tighter (Fig. 3*D*). The results also suggested that the cohesin head may serve as a DNA

anchor site. 2) Certain suppressor mutations of cohesin ATPase mutants and *rad21-I67F* were mapped in coiled coils emerging from the head, so that they are supposed to distort interactions between coiled coils and other subunits (Rad21/SCC1 and Mis4/SCC2/NIPBL) associated. One possible interpretation is that ATP-driven conformational changes may open closed coiled coils at the head as illustrated in Fig. 4*H*. 3) Suppressors in coiled coils around break sites indicate that structural changes may happen at break sites in coiled coils after ATP hydrolysis to reduce coiled-coil probabilities (Fig. 5*E*).

Taken together, we propose that Mis4/SCC2/NIPBL and DNA may stimulate cohesin ATPase activity (20–22) to drive a series of conformation changes at coiled coils emerging from the head to distort interactions between coiled coils and associated subunits (Rad21/SCC1 and Mis4/SCC2/NIPBL) to open closed coiled coils at the head and to extend coiled coils around break sites. These whole processes may bring DNA elements that are far from each other in linear distance together, which results in DNA loop formation and/or extrusion (Fig. 6).

Materials and Methods

Strains, Plasmids, and Media. The *S. pombe* haploid wild-type strain *972h*$^-$ was used as the host strain for isolation of Psm1/SMC1 and Psm3/SMC3 ATPase ts mutants. A pBluescript plasmid containing a hygromycin-resistance antibiotic marker was used for construction of various targeting vectors. Vectors with the Psm1/Psm3 wild-type open reading frame (ORF) integrated upstream of the antibiotic marker and ∼500-bp sequences after the Psm1/Psm3 ORF integrated downstream of the antibiotic marker were constructed and used as PCR templates for targeted saturation mutagenesis.

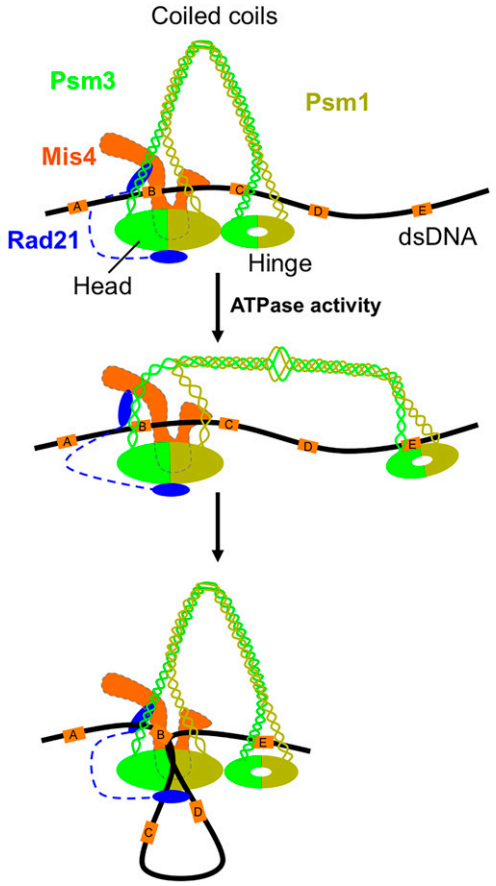

Fig. 6. Potential ATP-driven conformational changes. Cohesin loader Mis4/SCC2/NIPBL loads cohesin onto chromatin and arched coiled coils hold chromatin. ATPhydrolysis in the cohesin ATPase domains would trigger several structural changes: (1) to enhance DNA binding by the head domain, (2) to open coiled coils at the headthrough destabilizing the interactions of coiled coils with Rad21N and Mis4C, (3) to temporarily extend the folded coiled coils and separate the hinge from the head. Then, coiled coils fold back again to bring the head and hinge together, which also brings DNA elements that are far away proximal. *A*–*E* indicate five DNA elements in the genome.

A series of site-directed, PCR-based mutagenesis was then performed to introduce random "NNN" (encoding one amino acid) into the Psm1/Psm3 wild-type ORF to substitute each amino acid of "LSGG" in the signature motif (or the conserved "L" in the D loop) of the Psm1/Psm3 ATPase domain (Fig. 1*A*), using the two-step PCR protocol described in ref. 59 with three modifications: 1) Only the forward primer of the partially complementary primer pairs, designed to introduce random NNN into the Psm1/Psm3 wild-type ORFs, contains random NNN in its 3′ protrusion. 2) In the current work, not only the corresponding ORFs, but also the hygromycin-resistant antibiotic marker, and the 500-bp DNA sequences after the corresponding ORFs, were amplified by the PCRs. 3) In order to exclude potential nonspecific PCR bands, the first PCR products were purified by gel extraction instead of PCR cleanup. The final PCR products containing mutated Psm1/Psm3 ORFs, the hygromycin-resistance antibiotic marker, and DNA sequences after the Psm1/Psm3 ORF, were transformed into wild-type strain *972h*$^-$, followed by incubation on YPD agar plates containing hygromycin (500 μg/mL) for 5 d at 26 °C. Colonies (integrants) were picked and streaked on YPD plates to screen for ts mutants. Two copies were prepared for each colony, one copy was incubated at 26 °C and the other at 37 °C. Three days later, growth conditions of each colony at each temperature were compared. Ts mutants that grew at 26 °C, but not at 37 °C, were selected, and their responsible mutations were identified by targeted sequencing of the mutated region in Psm1/Psm3 gene sequences.

Suppressor Screening, Next-Generation Sequencing, and Suppressor Identification. The *psm1-L1132T*, *psm1-L1166N*, and *psm3-S1098A* strains were inoculated into YPD medium and cultured overnight. The 1×10^7, 5×10^7, and 1×10^7 cells were spread onto five YPD agar plates for *psm1-L1132T*, *psm1-L1166N*, and *psm3-S1098A*, respectively (2×10^6 cells/plate for *psm1-L1132T*, 1×10^7 cells/plate for *psm1-L1166N*, and 2×10^6 cells/plate for *psm3-S1098A*). The YPD agar plates were then incubated at restrictive temperatures (37 °C for *psm1-L1132T*, 36 °C for *psm1-L1166N*, and 37 °C for *psm3-S1098A*) for 4∼6 d for colonies to grow up. In total, 240, 320, and 320 survivor colonies were picked up for *psm1-L1132T*, *psm1-L1166N*, and *psm3-S1098A*, respectively. They were streaked on YPD agar plates for 4 d, and then stored in −80 °C.

Next-generation sequencing and suppressor identification followed the suppressor screening protocols described in ref. 36 with two modifications: 1) In the previous study, revertants (survivor strains) were divided into groups and each group contains 10 revertants. Genomic DNAs from each of the 10 survivor strains were extracted and then equal amount of genomic DNAs from each of the 10 survivor strains in the group were mixed together as a genomic DNA pool for next-generation sequencing. In the current study, we first mixed together equal amounts of cells from each of the 10 strains in the group, then genomic DNAs of the pooled cells were extracted for next-generation sequencing. 2) A DNBseq platform with paired-end (2 × 150 bp) runs was used instead of the Illumina HiSeq 2000 sequencing system.

Targeted Saturation Mutagenesis Followed by Suppressor Screen. A pBluescript plasmid containing a nourseothricin sulfate (or clonNAT) resistance antibiotic marker was used for construction of targeting vectors. Vectors with corresponding ORFs integrated upstream of the antibiotic marker and ∼500-bp sequences after the corresponding ORFs integrated downstream of the antibiotic marker were constructed and used for saturation mutagenesis. A series of site-directed PCR-based mutagenesis was then performed to introduce random NNN (encoding one amino acid) into the corresponding ORFs to replace each, but only one amino acid in the targeted regions. Equal amounts of each PCR product were mixed together to generate a mutation library for each targeted region. These mutation libraries were then transformed into corresponding ts mutants, streaked onto YPD plates containing clonNAT (200 μg/mL), and incubated at the restrictive temperature for 6 d. Revertants, each containing a single amino acid substitution in the targeted regions, were isolated. Their responsible single amino acid substitutions were identified by targeted sequencing of the mutated regions.

Prediction of Coiled-Coil Probabilities. Wild-type Psm1/SMC1 and Psm3/SMC3 protein sequences were downloaded from the PomBase database (https://www.pombase.org/) (60). Coiled-coil probabilities of wild-type Psm1/SMC1 and Psm3/SMC3 were calculated using MARCOIL (37) integrated into the MPI Bioinformatics Toolkit (https://toolkit.tuebingen.mpg.de/tools/marcoil) (61, 62).

Calculation of Mean Relative Hydrophobicity, Mean Relative Molecular Weights, and Mean Relative Coiled-Coil Probabilities. Kyte–Doolittle hydropathy scores of the 20 amino acids (63) were used for the calculation. The relative hydrophobicity scale of every single amino acid substitution was calculated using the formula: Relative hydrophobicity scale = hydrophobicity scale of mutant allele − hydrophobicity scale of wild-type allele. Mean relative hydrophobicity scale at every amino acid position in Psm1-CCN and Psm3-CCN was then calculated as the sum of the relative hydrophobicity scales of every single amino acid substitution identified at that position divided by the number of substitutions at the position.

The relative molecular weight of every single amino acid substitution in Psm3-BS, which was identified as a suppressor mutation of the Psm3/SMC3 ATPase ts mutant psm3-*S1098A*, was calculated using the formula: Relative molecular weight = molecular weight of mutant allele − molecular weight of wild-type allele. Mean relative molecular weight at every amino acid position in Psm3-BS was then calculated as the sum of relative molecular weights of all single amino acid substitutions identified at that position divided by the number of single amino acid substitutions at the position.

Mean relative coiled-coil probability at each amino acid position in Psm3-BS was calculated in a similar way as mean relative molecular weight. The coiled-coil probability of every Psm3/SMC3 mutant with a single amino acid substitution in Psm3-BS, which was identified as a suppressor mutation of the Psm3/SMC3 ATPase ts mutant psm3-*S1098A*, was calculated using the mutant Psm3/SMC3 protein sequence by replacing the wild-type amino acid with the corresponding mutant amino acid. The relative coiled-coil probability of every Psm3/SMC3 mutant with a single amino acid substitution in Psm3-BS was calculated using the formula: Relative coiled coil probability = coiled-coil probability of mutant allele − coiled-coil probability of the wild-type allele. Mean relative coiled-coil probability at every amino acid position in Psm3-BS was then calculated as the sum of relative coiled-coil probabilities of every single amino acid substitution identified at that position divided by the number of single amino acid substitutions at that position.

Calculation of Frequency of the 20 Amino Acids in Mutant Alleles. Frequencies of the 20 amino acids in mutant alleles obtained in Psm1-CCN or Psm3-CCN were calculated using the formula: Frequency of each of the 20 amino acids in the mutant allele = quantitative number of revertants with one wild-type amino acid in the particular domain (Psm1-CCN or Psm3-CCN) mutated to the mutant amino acid divided by the number of codons of the mutant amino acid.

Data Availability. The sequencing data reported in this paper have been deposited in the National Center for Biotechnology Information BioProject database (https://www.ncbi.nlm.nih.gov/bioproject, accession no. PRJNA846538).

ACKNOWLEDGMENTS. We thank Dr. Steven D. Aird for technical editing. Generous support from Okinawa Institute of Science and Technology Graduate University is gratefully acknowledged.

Author affiliations: [a]G0 Cell Unit, Okinawa Institute of Science and Technology Graduate University, Onna-son, Okinawa 904-0495, Japan; and [b]Institute for Quantitative Biosciences, University of Tokyo, Tokyo, 113-0032 Japan

1. F. Uhlmann, SMC complexes: From DNA to chromosomes. *Nat. Rev. Mol. Cell Biol.* **17**, 399–412 (2016).
2. S. Yatskevich, J. Rhodes, K. Nasmyth, Organization of chromosomal DNA by SMC complexes. *Annu. Rev. Genet.* **53**, 445–482 (2019).
3. P. Arumugam *et al.*, ATP hydrolysis is required for cohesin's association with chromosomes. *Curr. Biol.* **13**, 1941–1953 (2003).
4. C. H. Haering, J. Löwe, A. Hochwagen, K. Nasmyth, Molecular architecture of SMC proteins and the yeast cohesin complex. *Mol. Cell* **9**, 773–788 (2002).
5. A. Lammens, A. Schele, K. P. Hopfner, Structural biochemistry of ATP-driven dimerization and DNA-stimulated activation of SMC ATPases. *Curr. Biol.* **14**, 1778–1782 (2004).
6. K. P. Hopfner *et al.*, Structural biology of Rad50 ATPase: ATP-driven conformational control in DNA double-strand break repair and the ABC-ATPase superfamily. *Cell* **101**, 789–800 (2000).
7. R. Palou *et al.*, Condensin ATPase motifs contribute differentially to the maintenance of chromosome morphology and genome stability. *PLoS Biol.* **16**, e2003980 (2018).
8. R. Ladurner *et al.*, Cohesin's ATPase activity couples cohesin loading onto DNA with Smc3 acetylation. *Curr. Biol.* **24**, 2228–2237 (2014).
9. T. G. Gligoris *et al.*, Closing the cohesin ring: Structure and function of its Smc3-kleisin interface. *Science* **346**, 963–967 (2014).
10. C. H. Haering *et al.*, Structure and stability of cohesin's Smc1-kleisin interaction. *Mol. Cell* **15**, 951–964 (2004).
11. T. L. Higashi *et al.*, A structure-based mechanism for DNA entry into the cohesin ring. *Mol. Cell* **79**, 917–933.e9 (2020).
12. P. J. Huis in 't Veld *et al.*, Characterization of a DNA exit gate in the human cohesin ring. *Science* **346**, 968–972 (2014).
13. Y. Li *et al.*, Structural basis for Scc3-dependent cohesin recruitment to chromatin. *eLife* **7**, e38356 (2018).
14. M. B. Roig *et al.*, Structure and function of cohesin's Scc3/SA regulatory subunit. *FEBS Lett.* **588**, 3692–3702 (2014).
15. Z. Shi, H. Gao, X. C. Bai, H. Yu, Cryo-EM structure of the human cohesin-NIPBL-DNA complex. *Science* **368**, 1454–1459 (2020).
16. R. Ciosk *et al.*, Cohesin's binding to chromosomes depends on a separate complex consisting of Scc2 and Scc4 proteins. *Mol. Cell* **5**, 243–254 (2000).
17. K. Furuya, K. Takahashi, M. Yanagida, Faithful anaphase is ensured by Mis4, a sister chromatid cohesion molecule required in S phase and not destroyed in G1 phase. *Genes Dev.* **12**, 3408–3418 (1998).
18. W. C. Chao *et al.*, Structure of the cohesin loader Scc2. *Nat. Commun.* **8**, 13952 (2017).
19. S. Kikuchi, D. M. Borek, Z. Otwinowski, D. R. Tomchick, H. Yu, Crystal structure of the cohesin loader Scc2 and insight into cohesinopathy. *Proc. Natl. Acad. Sci. U.S.A.* **113**, 12444–12449 (2016).
20. Y. Kim, Z. Shi, H. Zhang, I. J. Finkelstein, H. Yu, Human cohesin compacts DNA by loop extrusion. *Science* **366**, 1345–1349 (2019).
21. Y. Murayama, F. Uhlmann, Biochemical reconstitution of topological DNA binding by the cohesin ring. *Nature* **505**, 367–371 (2014).
22. N. J. Petela *et al.*, Scc2 is a potent activator of cohesin's ATPase that promotes loading by binding Scc1 without Pds5. *Mol. Cell* **70**, 1134–1148.e7 (2018).
23. A. Matityahu, I. Onn, A new twist in the coil: Functions of the coiled-coil domain of structural maintenance of chromosome (SMC) proteins. *Curr. Genet.* **64**, 109–116 (2018).
24. O. Orgil, H. Mor, A. Matityahu, I. Onn, Identification of a region in the coiled-coil domain of Smc3 that is essential for cohesin activity. *Nucleic Acids Res.* **44**, 6309–6317 (2016).
25. T. Sutani, M. Yanagida, DNA renaturation activity of the SMC complex implicated in chromosome condensation. *Nature* **388**, 798–801 (1997).
26. L. Truebestein, T. A. Leonard, Coiled-coils: The long and short of it. *BioEssays* **38**, 903–916 (2016).
27. V. M. Waldman, T. H. Stanage, A. Mims, I. S. Norden, M. G. Oakley, Structural mapping of the coiled-coil domain of a bacterial condensin and comparative analyses across all domains of life suggest conserved features of SMC proteins. *Proteins* **83**, 1027–1045 (2015).
28. F. Bürmann *et al.*, A folded conformation of MukBEF and cohesin. *Nat. Struct. Mol. Biol.* **26**, 227–236 (2019).
29. A. Matityahu, I. Onn, Hit the brakes–A new perspective on the loop extrusion mechanism of cohesin and other SMC complexes. *J. Cell Sci.* **134**, jcs247577 (2021).
30. X. Xu *et al.*, Suppressor mutation analysis combined with 3D modeling explains cohesin's capacity to hold and release DNA. *Proc. Natl. Acad. Sci. U.S.A.* **115**, E4833–E4842 (2018).
31. P. Arumugam, T. Nishino, C. H. Haering, S. Gruber, K. Nasmyth, Cohesin's ATPase activity is stimulated by the C-terminal Winged-Helix domain of its kleisin subunit. *Curr. Biol.* **16**, 1998–2008 (2006).
32. A. M. O. Elbatsh *et al.*, Cohesin releases DNA through asymmetric ATPase-driven ring opening. *Mol. Cell* **61**, 575–588 (2016).
33. Z. K. Boswell, M. D. Canny, T. A. Buschmann, J. Sang, M. P. Latham, Adjacent mutations in the archaeal Rad50 ABC ATPase D-loop disrupt allosteric regulation of ATP hydrolysis through different mechanisms. *Nucleic Acids Res.* **48**, 2457–2472 (2020).
34. G. Çamdere, V. Guacci, J. Stricklin, D. Koshland, The ATPases of cohesin interface with regulators to modulate cohesin-mediated DNA tethering. *eLife* **4**, e11315 (2015).
35. N. Nakazawa, O. Arakawa, M. Ebe, M. Yanagida, Casein kinase II-dependent phosphorylation of DNA topoisomerase II suppresses the effect of a catalytic topo II inhibitor, ICRF-193, in fission yeast. *J. Biol. Chem.* **294**, 3772–3782 (2019).
36. X. Xu, L. Wang, M. Yanagida, Whole-genome sequencing of suppressor DNA mixtures identifies pathways that compensate for chromosome segregation defects in *Schizosaccharomyces pombe*. *G3 (Bethesda)* **8**, 1031–1038 (2018).
37. M. Delorenzi, T. Speed, An HMM model for coiled-coil domains and a comparison with PSSM-based predictions. *Bioinformatics* **18**, 617–625 (2002).
38. R. Straussman, A. Ben-Ya'acov, D. N. Woolfson, S. Ravid, Kinking the coiled coil–negatively charged residues at the coiled-coil interface. *J. Mol. Biol.* **366**, 1232–1242 (2007).
39. S. Gruber, C. H. Haering, K. Nasmyth, Chromosomal cohesin forms a ring. *Cell* **112**, 765–777 (2003).
40. A. Sakai, K. Hizume, T. Sutani, K. Takeyasu, M. Yanagida, Condensin but not cohesin SMC heterodimer induces DNA reannealing through protein-protein assembly. *EMBO J.* **22**, 2764–2775 (2003).
41. C. H. Haering, A. M. Farcas, P. Arumugam, J. Metson, K. Nasmyth, The cohesin ring concatenates sister DNA molecules. *Nature* **454**, 297–301 (2008).
42. D. Ivanov, K. Nasmyth, A topological interaction between cohesin rings and a circular minichromosome. *Cell* **122**, 849–860 (2005).
43. S. Hauf, I. C. Waizenegger, J. M. Peters, Cohesin cleavage by separase required for anaphase and cytokinesis in human cells. *Science* **293**, 1320–1323 (2001).
44. F. Uhlmann, F. Lottspeich, K. Nasmyth, Sister-chromatid separation at anaphase onset is promoted by cleavage of the cohesin subunit Scc1. *Nature* **400**, 37–42 (1999).
45. F. Uhlmann, D. Wernic, M. A. Poupart, E. V. Koonin, K. Nasmyth, Cleavage of cohesin by the CD clan protease separin triggers anaphase in yeast. *Cell* **103**, 375–386 (2000).

46. S. Uzawa, I. Samejima, T. Hirano, K. Tanaka, M. Yanagida, The fission yeast cut1+ gene regulates spindle pole body duplication and has homology to the budding yeast ESP1 gene. *Cell* **62**, 913–925 (1990).
47. S. H. Yoshimura *et al.*, Condensin architecture and interaction with DNA: Regulatory non-SMC subunits bind to the head of SMC heterodimer. *Curr. Biol.* **12**, 508–513 (2002).
48. M. Beasley, H. Xu, W. Warren, M. McKay, Conserved disruptions in the predicted coiled-coil domains of eukaryotic SMC complexes: Implications for structure and function. *Genome Res.* **12**, 1201–1209 (2002).
49. X. Xu, M. Yanagida, Suppressor screening reveals common kleisin-hinge interaction in condensin and cohesin, but different modes of regulation. *Proc. Natl. Acad. Sci. U.S.A.* **116**, 10889–10898 (2019).
50. F. Bürmann, L. F. H. Funke, J. W. Chin, J. Löwe, Cryo-EM structure of MukBEF reveals DNA loop entrapment at chromosomal unloading sites. *Mol. Cell* **81**, 4891–4906.e8 (2021).
51. N. J. Petela *et al.*, Folding of cohesin's coiled coil is important for Scc2/4-induced association with chromosomes. *eLife* **10**, e67268 (2021).
52. Y. Murayama, F. Uhlmann, DNA entry into and exit out of the cohesin ring by an interlocking gate mechanism. *Cell* **163**, 1628–1640 (2015).
53. M. T. Hons *et al.*, Topology and structure of an engineered human cohesin complex bound to Pds5B. *Nat. Commun.* **7**, 12523 (2016).
54. L. Käshammer *et al.*, Mechanism of DNA end sensing and processing by the Mre11-Rad50 complex. *Mol. Cell* **76**, 382–394.e6 (2019).
55. T. Mizuguchi *et al.*, Cohesin-dependent globules and heterochromatin shape 3D genome architecture in *S. pombe*. *Nature* **516**, 432–435 (2014).
56. I. F. Davidson, J. M. Peters, Genome folding through loop extrusion by SMC complexes. *Nat. Rev. Mol. Cell Biol.* **22**, 445–464 (2021).
57. A. L. Sanborn *et al.*, Chromatin extrusion explains key features of loop and domain formation in wild-type and engineered genomes. *Proc. Natl. Acad. Sci. U.S.A.* **112**, E6456–E6465 (2015).
58. I. F. Davidson *et al.*, DNA loop extrusion by human cohesin. *Science* **366**, 1338–1345 (2019).
59. X. Xu, M. Yanagida, Isolation of fission yeast condensin temperature-sensitive mutants with single amino acid substitutions targeted to hinge domain. *G3 (Bethesda)* **9**, 1777–1783 (2019).
60. V. Wood *et al.*, PomBase: A comprehensive online resource for fission yeast. *Nucleic Acids Res.* **40**, D695–D699 (2012).
61. F. Gabler *et al.*, Protein sequence analysis using the MPI bioinformatics toolkit. *Curr. Protoc. Bioinformatics* **72**, e108 (2020).
62. L. Zimmermann *et al.*, A completely reimplemented MPI bioinformatics toolkit with a new HHpred server at its core. *J. Mol. Biol.* **430**, 2237–2243 (2018).
63. J. Kyte, R. F. Doolittle, A simple method for displaying the hydropathic character of a protein. *J. Mol. Biol.* **157**, 105–132 (1982).